HOST UNIVERSITY: Ghent University

FACULTY: Faculty of Engineering

DEPARTMENT: Department of Flow, Heat and Combustion Mechanics

PARTNER UNIVERSITY: The University of Maryland

FACULTY: School of Engineering

DEPARTMENT: Department of Fire Protection Engineering

Academic Year 2015-2016

A Numerical Investigation of Spray-Plume Interactions

Sami Takieddin

Promoter: Prof. Bart Merci

Supervisor: Prof. Arnaud Trouvé

Master thesis submitted in the Erasmus Mundus Study Programme

International Master of Science in Fire Safety Engineering

Disclaimer

This thesis is submitted in partial fulfilment of the requirements for the degree of *The International Master of Science in Fire Safety Engineering (IMFSE)*. This thesis has never been submitted for any degree or examination to any other University/programme. The author declares that this thesis is original work except where stated. This declaration constitutes an assertion that full and accurate references and citations have been included for all material, directly included and indirectly contributing to the thesis. The author gives permission to make this master thesis available for consultation and to copy parts of this master thesis for personal use. In the case of any other use, the limitations of the copyright have to be respected, in particular with regard to the obligation to state expressly the source when quoting results from this master thesis. The thesis supervisor must be informed when data or results are used.

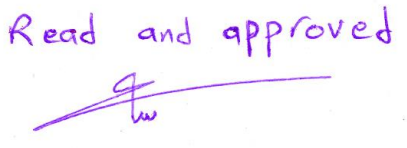

29/04/2016

Abstract

Water sprays are considered one of the most reliable fire suppression systems because of the tremendous effectiveness they have in multi applications. Fire sprinklers are one of the water spray systems that have been used widely over years. Although the mechanisms in which fire sprinkler sprays suppress fires are easily identified, the factors that govern the interaction between the spray and the fire are poorly investigated. The present work uses the CFD software FireFOAM to establish a numerical simulation for the plume-sprinkler interaction. Besides, some numerical results are validated through experimental measurements. The results show that the size of droplets influences the plume and the delivered water into it. Also, it is shown that numerical resolution is an essential requirement for having an acceptable level of error. It is found that the effect of plume speed is in good agreement with experimental results. Raising the temperature increases the water flux at the position of the plume, while droplets' evaporation is found to have an insignificant effect on water flux. Placing the plume in different positions shows that it decreases the delivered water to 30-60% of its original value. Separately, it is shown that sprinkler spray decreases the plume velocity and makes it bent.

Abstract (Arabic)

خلاصة

يعتبر استخدام رذاذ الماء من الوسائل ذات الكفاءة العالية لإطفاء الحريق في تطبيقات مختلفة، ومن ضمن هذه الأنظمة توجد مرشات الماء المستخدمة بشكل واسع على مدى السنين. إن العوامل المتحكمة في التأثير المتبادل بين رذاذ الماء وعمود النار غير محددة بشكل كافي على الرغم من سهولة فهم طريقة عمل هذه المرشات في إطفاء الحرائق. تم في هذا البحث استخدام برنامج حاسوبي لديناميك الموائع يدعى FireFOAM لإجراء محاكاة للتأثير المتبادل بين الرذاذ و دخان النار، كما تم استخدام نتائج تجريبية للتحقق من صحة نتائج البرنامج، وقد أظهرت النتائج تأثير حجم قطرات الماء على معدل وصولها لمكان النار كما وجد أنها تؤثر بشكل كبير على سرعة الدخان. من ناحية أخرى فقد بينت الدراسة أهمية اختيار بارامترات المحاكاة بشكل دقيق للحصول على حد مقبول من الخطأ، ووجد أن نتائج تأثير سرعة الدخان مطابقة بشكل كبير لما تم الحصول عليه تجريبياً. كما تبين أن زيادة درجة حرارة الدخان المستخدم تعمل على زيادة معدل وصول الماء لمكان النار، وإن هذا المعدل لا يتأثر بشكل كبير نتيجة تبخر الماء، كما أن كمية معدل وصول الماء لمكان النار تتراوح بين 30% و 60% من قيمتها عند التشغيل بدون وجود نار. تم التوصل لخلاصة أن رذاذ مرش الماء يؤثر بشكل كبير على سرعة الدخان حيث أنها تنخفض وتميل مبتعدة عن المرش.

Table of Contents

List of Figures

List of Tables

List of acronyms and symbols

b half width of the plume

C sprinkler constant

CVF drop size volume flux cumulative distribution function

d drop diameter

dt time step

dx grid size

D_0 orifice diameter

dv_{50} median drop size

f_D drag force

$f_{r,i}$ true local measurement

$f_{x,i}$ tested local measurement

K sprinkler K-factor

n droplet number density

N number of measurements

$\dot{N}$ Lagrangian particle injection rate

P pressure

R radius of the sphere

t_s characteristic time

u plume velocity

U_{jet} jet velocity

U_c characteristic velocity

V drops velocity

V_{spray} spray volume

We Weber number

x_c characteristic length

z vertical distance in equations

α entrainment coefficient

δ_x error

θ elevation angle

ρ water density

ρ_{diff} buoyancy

σ surface tension

ϒ drop size distribution width

ψ azimuthal angle

1 Introduction & objectives

Water spray based fire suppression systems are increasingly used because they are highly effective at extinguishing fires. There are four mechanisms by which a water spray may supress a fire: by cooling of the burning surface (fuel cooling), by cooling of the hot gases (flame cooling), by oxygen displacement, or by pre-wetting the unburnt fuel [1].

There are two primary types of water based fire suppression sprays: fire sprinklers and water mist. The two systems are primarily distinguished by the size distribution of spray droplets [2]. Water mist sprays are primarily composed of droplets with diameters less than $100\ \mu m$, while sprinkler sprays are primarily composed of droplets with diameters greater than $100\ \mu m$. This droplet size difference lends itself to two different primary suppression mechanisms: flame cooling for the water mist systems and fuel cooling for sprinkler systems [3], [4]. The smaller drops of water mist systems are quick to evaporate, extracting heat from the hot gases, but lack the momentum to penetrate to the fuel surface. The large drops of fire sprinkler sprays are far slower to evaporate, extracting less heat from the air, but are consequently better able to penetrate to, and cool, the fuel surface [1].

As a result, a major concern in the design of fire sprinklers is their ability to successfully deliver water to the protected surfaces. In order to deliver the water spray to the burning surface, the spray must penetrate through the fire plume, overcoming the buoyant upward momentum [1]. Understanding the interaction between the plume and the spray is critical to the design of fire sprinklers and their implementation in fire suppression systems.

Fire sprinklers have been increasingly used over the last 100 years. Figure 1 shows a diagram of a D3-type spray nozzle, the fire sprinkler used in this study. There are many types of sprinklers, but all generally share similar features [5]: the inlet (by which a water jet enters), and frame arms, a boss and a deflector, which deflect the incoming jet and form a series of sheets, as seen in Figure 2, which eventually atomize and form the initial spray [6]. This unusual atomization method leads to strong spatial variations in the initial spray, and a number of studies have sought to characterize this variation.

Ren and Marshall [6]–[8] carried out an experimental study at the University of Maryland to characterize the initial spray from fire suppression nozzles. They noted that the unstable and chaotic physical atomization mechanisms make the prediction of the initial spray of fire suppression nozzles more challenging. In addition, the variation in the design among them adds more complexity when characterising the nozzles. The measurements of the multiphase breakup region, the small scale free surface physics modelling, and the strong coupling with fire environment dynamic are the main reasons behind not having an exact description of the initial spray [8].

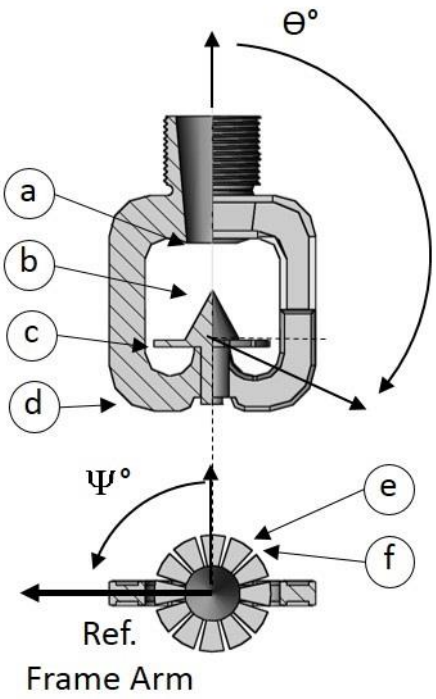

Figure 1 A partial cross section of a D3 spray nozzle consisting of: a. inlet, b. boss, c. deflector, d. frame arms, e. tines, f. slots [5]

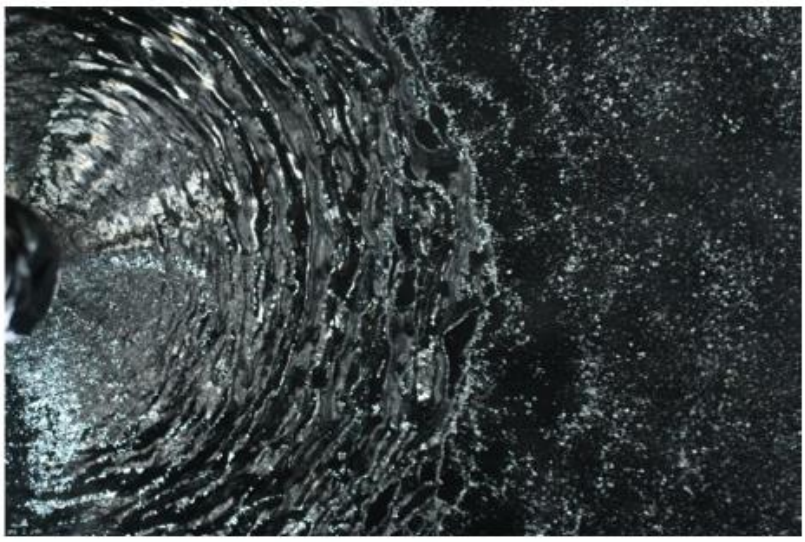

Figure 2 Top view photograph of a sheet during the breakup process of a sprinkler spray [6]

Work by Myers [9] shows that the initial sprinkler spray may be described in spherical coordinates, with spray properties varying across a measurement surface with radius, R, azimuthal angle, ψ, and elevation angle, θ, as seen in Figure 3. Zhou used a laser-based shadow-imaging system to study the sprinkler behaviour and he found that the sprinkler arms and the configuration of the deflector's tines and slots strongly affect the spatial distribution

of water volume flux, droplet size, and velocity of the spray [2]. A map of the near-field spray volume flux for a D3 type spray nozzle (the nozzle used in this study) may be seen in Figure 4. It can be seen that volume flux varies widely with angle, reflective of the tine and slot structure of the sprinkler head.

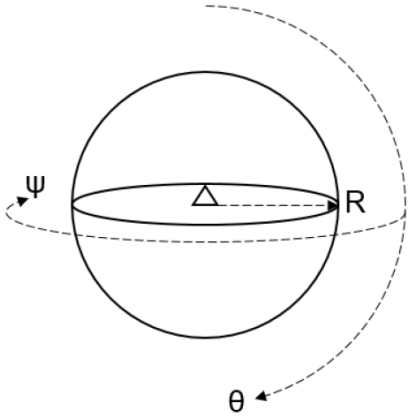

Figure 3 The initialization sphere, radius R, elevation angle θ, and azimuthal angle ψ [9]

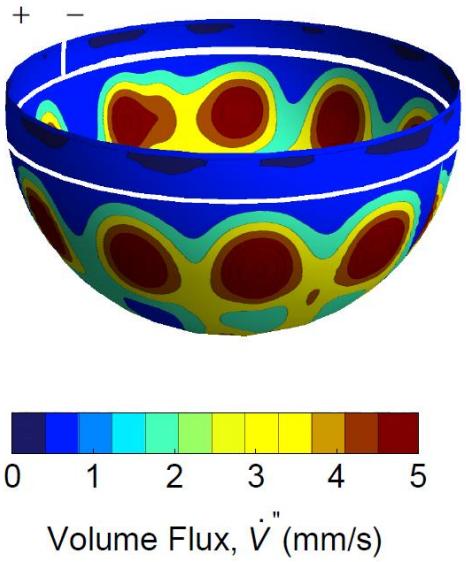

Figure 4 The non-uniform volume flux for the D3 spray nozzle used in this study [5]

Zhou [2] ,Ren [7] and Schwille [1] emphasized the finding by Yu [10] that the cumulative droplet-size distribution of the sprinklers is represented by a combination of log-normal and Rosin-Rammler distributions as seen in equation (1) which prescribe the starting spray conditions.

$$CVF(d) = \begin{cases} \frac{1}{2\pi}\int_0^d \frac{\gamma}{1.15\,d'}\, exp\left(-\frac{\left(\ln\left(\frac{d'}{d_{v50}}\right)\right)^2}{2(\frac{1.15}{\gamma})^2}\right) dd', & d < d_{v50} \\ 1 - exp^{-0.693(d/d_{v50})^{\gamma}}, & d > d_{v50} \end{cases} \quad (1)$$

Where γ is the distribution width parameter and d_{v50} is the volumetric median droplet diameter which has $CVF(d_{v50}) = 0.5$. Both d_{v50} and γ are functions of location. The median droplet diameter d_{v50} gives a picture of the overall droplets present in a control volume and it means that 50% of the cumulated droplet volume is from droplets that have diameters smaller than d_{v50}. It is also noted that there is no relationship between droplet size and velocity. However, there is a general correlation that shows a higher velocity for the larger droplets because small droplets lose their momentum faster than large droplets [2]. Figure 5 shows the correlation between the velocity and the size of the droplets. Also, the droplet velocity is affected more by the elevation angle than the azimuthal angle. On the other hand, the water flux strongly depends on the elevation angle, azimuthal angle, water pressure, and sprinkler type [2].

Researches done by Zhou [11] and Widmann [12] affirmed the earlier findings by Heskestad, and Dundas, that the droplet size varies inversely with 1/3-power of sprinkler operation pressure (Weber number). The proposed correlation by Heskestad is seen in equation (2).

$$\frac{d_{v50}}{D_0} = CWe^{-1/3} \quad (2)$$

Where D_0 is the orifice diameter, C is a sprinkler constant depends on its geometry, and We is Weber number defined in equation (3).

$$We = \rho D_0 \frac{U^2}{\sigma} \quad (3)$$

Where U is the maximum initial spray velocity, ρ is water density, and σ is surface tension.

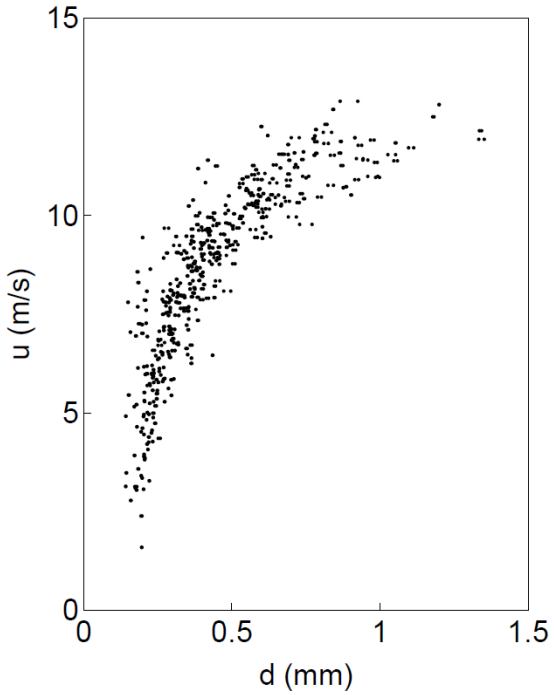

Figure 5 the drop size-velocity correlation for the sprinkler shown in figure 1 at Θ = 115° and Ψ = 245° [5]

Additionally, work by Zhou [2] investigated the far field drop size and velocity distributions. He found that the droplets' size in the spray centre is the largest, then it decreases to a minimum at 0.5 m from the centre, followed by a gradual increase with distance toward the outer edge of the sprinkler as seen in Figure 6. Also, he found that the radial distribution of the droplet velocity reaches its maximum near the centre of the sprinkler and then it decreases to the outer side of the spray. These results may be attributed to the slowing of drops by air drag, which is strongly dependent on drop size, as they move through the air.

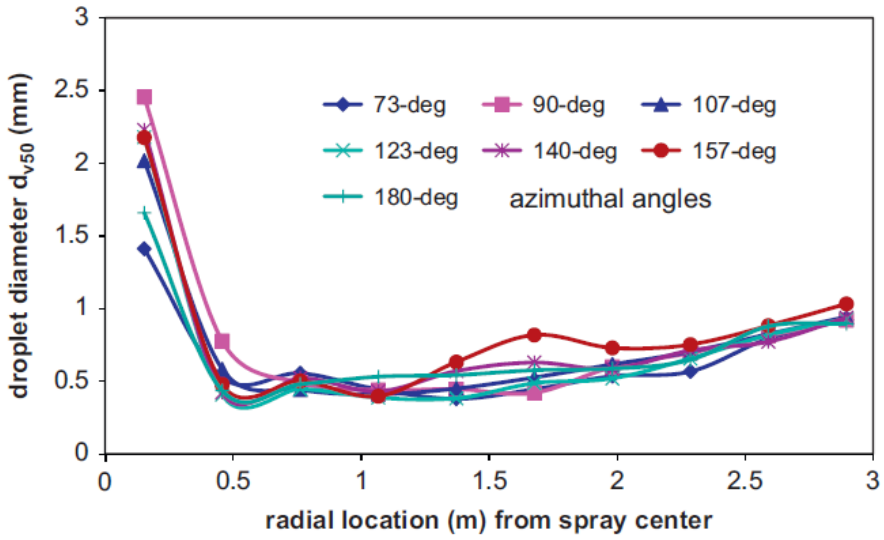

Figure 6 The radial distribution of volume median droplet diameter for different azimuthal angles [2]

Despite detailed studies of spray characteristics and dispersion, detailed information about the factors that affect the interaction between the spray and the plume are not available. Early studies done by Morton et al. [13] described the fluid motion in a fire plume by equations that have been used since the 1950s. However, the equations that describe the motion are not valid for fire suppression cases, because the interaction between the plume and the water droplets is not taken into account. Few researches have been done to investigate this interaction which is essential in improving fire suppression.

Schwille [1] focused on developing the equations by Morton et al. in order to include the effect of the spray momentum on the plume. He found that the spray droplets widen the plume and reduce its speed as they interact with each other. Schwille also concluded that the momentum interaction between the plume and the spray is critical for fire suppression. If the momentum of the spray is larger than the momentum of the plume, it is likely that the fire will be suppressed. In contrast, if the plume momentum overwhelms the spray momentum, it is unlikely that the droplets will penetrate the plum, therefore, the fire continues to grow.

Many assumptions and simplifications were introduced in Schwille model, but in general he found that droplets fall at their terminal velocities. Moreover, the largest droplets, which are affected least by evaporation, carry the majority of the water volume in the spray. The differential equations Schwille came up with are presented in equations (4), (5) and (6).

$$\frac{db}{dz} = 2\alpha - \frac{b\rho_{dif}}{2u^2} + \frac{bnf_D}{2u^2} \qquad (4)$$

$$\frac{du}{dz} = -\frac{\rho_{dif}}{u} - \frac{nf_D}{u} - \frac{2\alpha u}{b} \qquad (5)$$

$$\frac{d(\rho_{dif})}{dz} = -\frac{2\alpha\rho_{dif}}{b} \qquad (6)$$

Where z is the vertical distance, ρ_{dif} is the buoyancy, b is the half width of the plume, u is the velocity of the plume, α is the entrainment coefficient, n is the droplet number density, and f_D is the drag force. In his results he found a vertical position where the plume widens and its velocity goes to zero due to the balance between the upward and downward momentums from the plume and the spray respectively. This vertical position is called the 'interaction boundary'.

One of the earliest model that simulated the interaction between fire plumes and fire sprinkler sprays was developed by Nam [14], [15] using three different simulations that present the fire plume, the sprinkler spray and the interaction between them. He defined the required delivered density (RDD) and the actual delivered density (ADD) as the main factors to determine if the fire is suppressed or not. If ADD is larger than RDD, which is the amount needed to be delivered over the burning fuel to suppress the fire, then it is expected that the fire will be suppressed.

Nam [15] showed that for each sprinkler there is an optimal flow rate that delivers the highest penetration ratio in a specific flow range. Also, in order to have a higher penetration ratio, it is more effective to increase the droplet size than to increase the spray momentum, each at a time. However, Schwille [1] proved that it is not effective to increase the droplet size to prevent the fire from growing.

As described above, more efforts were done especially in the last decade due to the increase in numerical capabilities. Still, the fire extinguishing mechanism in fire sprinklers needs a lot of understanding especially in the interaction between the fire plume and the water spray that has a complex chemical and physical phenomenon. Hua et al. [16] have referred to this complexity and the lack of numerical modelling which is able to estimate the behaviour of water sprays and its effectiveness in a stage that can be used in the designing of different operating environments and fire types.

As a result of this shortage in information about the plume spray interaction, the University of Maryland and FM Global have started a common project using experimental and numerical studies in order to have more understanding on different cases. FM Global has developed an open CFD source code model called FireFOAM [17] based on another CFD source code called OpenFOAM [18]. FireFOAM is developed to facilitate as a tool to predict fire growth and fire suppression including a number of physical models (fluid mechanics, heat transfer, combustion, etc.) [19].

This project has two parts: the first is the experimental studies (some of them are summarized below) being done by A.W. Marshall, P.B. Sunderland, E.D. Link, J.P. White, and Stephen J. Jordan, while the second is the ongoing supporting CFD models being carried out by A. Trouvé, T.M. Myers, S. Vilfayeau, and J.P. White. FireFOAM software is being validated and developed through the two parts of the project.

More recent tests are being carried out by Link et al. [20], [21] at the University of Maryland in order to be able to resolve the spray dispersion by measurements and give a comprehensive data set for computer model validation. Link measured the initial spray (near-field) and near the floor (far-field) volume fluxes without the existence of a plume and he found that the volume flux is highly affected by sprinkler geometry details; frame arm, positioning, and slot/tine patterns [20]. In other words, each sprinkler has a unique initial volume flux regardless of the similarity in model and injection conditions. Therefore, in order to be able to validate computer models, detailed characterization of sprinkler injection conditions is needed.

Link et al. [21] has developed the previous experimental model. Preliminarily, Link introduced a challenge to the spray by adding a well-characterized upward air jet to work as a fire plume. He found that when plume's momentum is less than spray's momentum, and/or the terminal velocity of individual drops exceeds the velocity in the plume, then the penetration may occur. The penetration mechanisms and spray-plume interaction are characterized by

different penetration regimes through changing jet strength, spray strength, drop sizes, and jet locations. He measured the volume flux delivered to the floor by an array of four sprinklers in opposition of the air jet. The measurements were also taken by using a single sprinkler.

The present study performs as a part of the CFD modelling in the project between the University of Maryland and FM Global and it is dedicated to investigate the interaction between the plume and the spray. The carried out cases include changing of the spray and the plume. The spray is characterized as a monodispersed spray and as a polydispersed spray. The monodispersed spray includes the change of drop diameter. While in polydispersed spray cases, a variation in plume conditions is done. The plume speed, the temperature of the plume, and the position of the plume were examined. The results from experiments were used to validate the numerical results as applicable. Also, a check for resolution's effect was carried out to justify the choice of mesh size, time step, and spray resolutions.

The objectives of the present work are:

- Investigate the effect of drops' size on plume's speed and volume flux.
- Determine the correlation between the resolution and the error and find the appropriate mesh size, time step and spray resolutions to resolve the sprinkler-plume interaction quite well.
- Examine the effect of water evaporation on volume flux at different plume's temperature.
- Investigate the interaction between a polydispersed sprinkler spray and a cold plume with the variation of plume's speed and plume's position.
- Compare the results from experiments and simulations where applicable.

2 Methodology

2.1 Numerical solver

In the present work, a number of numerical simulations were done using the computational fluid dynamics fire model; FireFOAM which integrates a number of physical models in fluid mechanics, heat transfer, and combustion. It uses an object-oriented code structure, multi-physics modelling approaches, advanced meshing techniques and parallel computing [19]. Myers et al. [22] have verified the correct implementation of particle acceleration equation (the Basset, Boussinesq and Oseen (BBO)). They found that drop motion is governed entirely by gravity and spherical particle drag.

FireFOAM relies on an Eulerian-Lagrangian (EL) approach to capture sprinkler and water mist sprays. Here, the continuous phase (gaseous phase) is represented as an Eulerian field, while the dispersed phase (drops) are modelled using Lagrangian particle tracking. In particular, the gas phase is handled with an Eulerian Large Eddy Simulation (LES) model and the spray drops are handled using Lagrangian Discrete Droplet Model (DDM) [22],[23]. FireFOAM was found to accurately conserve spray mass, and accurately solve the Lagrangian equations of drop motion and of heat and mass transfer between the Lagrangian drops and the surrounding Eulerian domain [22].

In DDM, physical drops are bundled into numerical particles each of which is a representative of a number of physical drops. The trajectory of each particle is predicted by solving the Lagrangian equations of mass, momentum, and energy. This approach offers a computational and accuracy advantage over Eulerian models of the spray as the number of the Lagrangian equations that have to be solved is reduced. However, by this method, the water spread may be not adequate (less coverage) and the drop-to-drop interaction may be obscured [19].

Two different ways are available to initialize the spray, direct modelling of the atomization of the spray or measuring the initial spray in the near-field. The latter is used widely, as direct modelling is difficult to predict because of the aerodynamics instabilities and the interaction between drops [19]. Because of that, the initial sprinkler spray must be prescribed rather than predicted. So, the spray of the sprinkler is initialized on a sphere Figure 4 and it is assumed that all sheets and jets have been atomized completely inside the sphere, so after the sphere we only have a spray. If we specify the fire sprinkler spray sufficiently close to the injector, it will not yet have had the opportunity to interact with its surroundings. In this way, we may computationally investigate the impact of varying background conditions on fire sprinkler sprays and vice versa.

2.2 Numerical structure

As in OpenFOAM, the construction of the cases in FireFOAM should consist of three main folders: 0, constant, and system. This splitting gives the user more control on the simulation. The folder 0 contains the boundary and initial conditions for the variables. The constant folder

includes the characteristics of the mesh and the used models. In the system folder, running time, time step, integration schemes, and the solver are specified.

FireFOAM has its unique spray injection model “uniformSamplingSprinklerInjection” besides the injection models from OpenFOAM such as “coneInjection”. Both models were used in this study.

The model “uniformSamplingSprinklerInjection” allows to specify the spatially varying spray properties such as local volumetric flux normal to the initialization sphere. The characteristics of the sprinkler on the initialization sphere and droplets injection rate are specified through the subdirectory “constant\reactingCloud1Properties” which contains a reference to other subdirectory “XXXProperties” which also includes a reference to another directory “table_XXX”. The properties specified in “XXXProperties” are described in Table 1. While the remaining properties are specified in the “table_XXX” directory which has many subdirectories described in Table 2 [19]. In the appendix, an example of entries in the subdirectories “reactingCloud1Properties”, and “XXXProperties” are provided.

Table 1 Sprinkler properties listed in XXXProperties

Property	Description
sampleSize	Parcels injected per time step
tableDirectory	Directory that contains all listed sprinkler properties
SOI	Start of injection (when in the simulation particles begin to be injected)
duration	Duration of particle injection
parcelsPerSecond	Number of parcels injected per sprinkler per second
positionList	Sprinkler locations in the domain
direction	Direction corresponding to an elevation angle of 90 degrees
armDirection	Direction of (0,0) in elevation and azimuthal angle for sprinkler properties
radiusToSprinkler	Radius from the sprinkler to the initialization sphere

Table 2 Files in the table_XXX directory

File	Description
lookup.foam.header	Contains basic information about sprinkler flow, radius, and the number of azimuthal and elevation angles
lookup.foam.azi	Contains a scalar list of the azimuthal angle at each ordered pair of elevation and azimuthal angle
lookup.foam.ele	Contains a scalar list of the elevation angle at each ordered pair of elevation and azimuthal angle
lookup.foam.area	Contains a scalar list of the angular area at each ordered pair of elevation and azimuthal angle

lookup.foam.avgFlux	Contains a scalar list of the volumetric flux at each ordered pair of elevation and azimuthal angle

Besides the information in "table_XXX" directory, FireFOAM computes the average normal velocity V, and the volumetric median droplet diameter d_{v50} by equation (7) and equation (2) respectively [17].

$$V = U_{jet} \times 0.8 \qquad (7)$$

Where U_{jet}, is the jet velocity given in equation (8) in m/s, while 0.8 is the factor of momentum loss during atomization.

$$U_{jet} = \frac{K\sqrt{P}}{15\rho\pi D_0^2} \qquad (8)$$

Where K is the K-factor of the sprinkler specified in "lookup.foam.header" subdirectory and given in LPM/bar$^{0.5}$, P is the pressure in bar, ρ is water density in kg/m^3, and D_0 is orifice diameter in m. An example of entries in the subdirectory "lookup.foam.header" is provided is the appendix.

FireFOAM uses the information above to inject particles into the domain by following a specific procedure and using the initial properties specified in the subdirectory "reactingCloud1Properties". After injecting, the particles are tracked with a tracking algorithm and the mass, momentum, and energy change are updated each time step or grid cell that the particle passes through. The sub-models and post processing (particle collection) tools are also specified in "reactingCloud1Properties".

The sub-models handle the particles' interactions with the gas phase and the solid surfaces. The most important sub-models are: particleForces, dispersionModel, heatTransferModel, phaseChangeModel, radiation, and patchInteractionModel.

2.3 The configuration

The numerical domain used in this study is a simple configuration of the experimental facility at the University of Maryland. The experimental setup consists of an array of four sprinklers arranged in a square configuration measuring 2.65 m as seen in Figure 7 [21].

A plume represented by an air jet that flows through a square vent which side is 20 cm, and a series of water collection tubes, used for measurement of volume flux delivered 1.5 m below the sprinkler, may also be seen in Figure 7. The experiments done by Link [20], [21] showed the results for one sprinkler and for the array of the four sprinklers in the absence of the plume and with the existence of it.

The numerical domain is a one-meter-wide domain represents a diagonal part of the experimental facility as seen in Figure 8. The dimensions of the numerical domain are: the

length is 4 m, the height is 2 m, and the width is 1 m. The length is in the x-direction, the height is in the y-direction, and the width is in the z-direction (as default in FireFOAM). The points in X and Y directions are in positive values. However, the length has been extended 10 cm in the negative x-direction to allow the particles to be injected into the domain. The points in Z direction are in positive and negative values as the width is divided in half by the origin point as seen in Figure 9.

Unless mentioned differently, the injection sprinkler is positioned at (0, 1.5, 0), while the plume is centred at (1.87, 0, 0) which is the centre point of the experimental configuration as well.

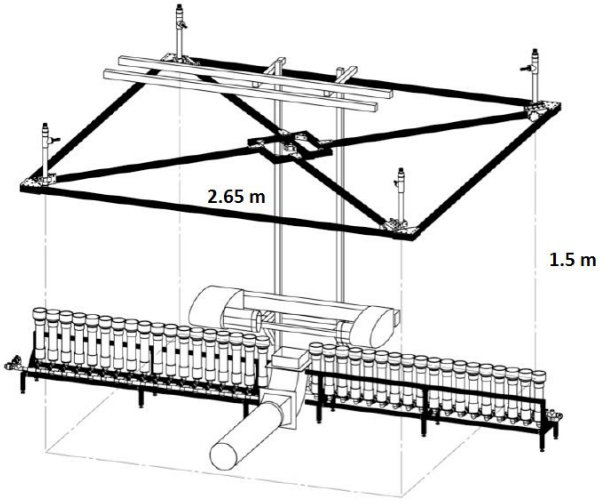

Figure 7 Drawing of the experimental facility showing the arrangement of the sprinklers, the water collection tubes, and the square plume [21]

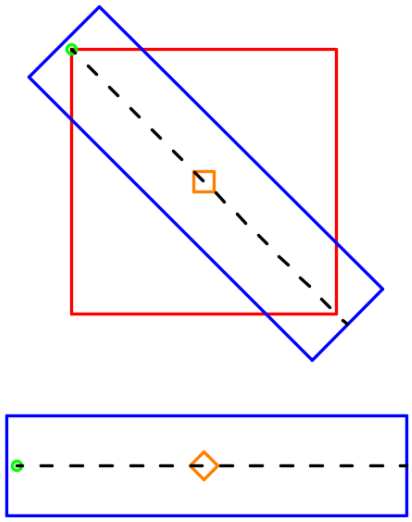

Figure 8 The numerical configuration used in the simulation (blue) compared to the experimental configuration (red) with the position of the plume (orange) ,the sprinkler (green), and the collectors' positions (dashed black)

2.4 Parameters' values

The characteristics of the plume and the sprinkler in the simulation were defined to match those in experiments. The sprinkler k-factor is 33.1 LPM/bar$^{0.5}$ and the water pressure in the sprinkler is 1.36 bar (yielding 0.64 kg/s), plume's velocity is 2.4 m/s (vertically), and its temperature is $298\ °K$ (unless mentioned differently). In experiments, the plume is represented by an air jet that flows through a square vent which side is 20 cm and centred in the middle of the configuration, so its vertices vary diagonally around the centre by 14 cm. However, as the numerical configuration was taken diagonally from the experimental configuration and we are interested in the linear dimension along x-direction, the plume was represented in the simulation by a square that has a 28-cm side between 1.73 and 2.01 in the x-direction and between -0.14 and 0.14 in the z-direction. Nevertheless, this change in the dimensions of the plume without changing the velocity of it, makes the total momentum and the mass flow rate of the plume bigger. As a result, the water flux distribution on the ground could be different.

A number of 32 collectors has been positioned on the ground along the x-direction. Each of them has the length of 12.5 cm and a width of 10 cm and centred on the x-axis. Figure 9 shows the configuration of the domain (from ParaView), the plume base is coloured red.

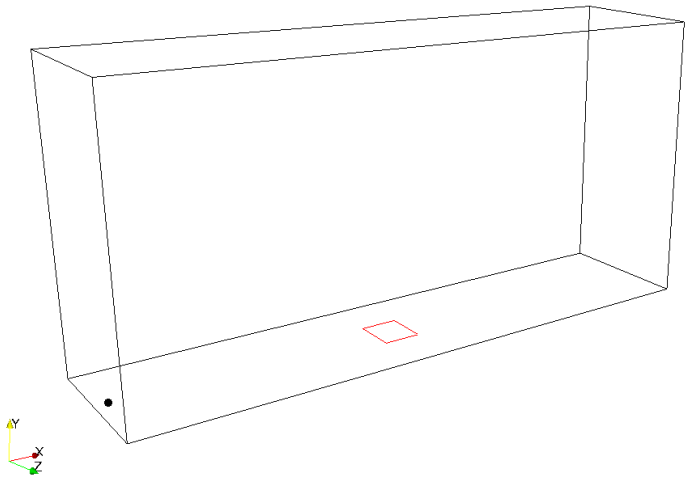

Figure 9 The numerical configuration of the domain

In FireFOAM files, the total number of azimuthal angles was specified to be 360, while the total number of elevation angles was 91. The radius of the sphere used in this study was 0.05 m, this sphere has been characterized through measurements of the near-field volume flux done in the spray lab at the University of Maryland with a Spatially-resolved Spray Scanning System (4S) using a typical pendant-type sprinkler head. Figure 4 shows the angular variation of water flux on the sphere which illustrates the effect of tines and slots on this flux. The

measurements give the value of volume flux at each elevation and azimuthal angle. The same working conditions were employed in simulations and experiments. The simulation time in all the studied cases was 20 seconds.

The velocity of droplets calculated by FireFOAM using equation (7) is 12.3 m/s, while in experiments it was 12.9 m/s. The median droplet diameter calculated from equation (2) is 0.0005 m, while it was 0.0006 m is experiments. The distribution width γ is 2 while in experiments it was 2.3. Table 3 summarizes the values of the spray in the simulation and experiments. The "lookup.foam.avgFlux" subdirectory contains a list of volume flux angular variations taken from measurements shown in Figure 4.

Table 3 Spray's parameters

Parameter	Experiment	Simulation
K-factor (LPM/bar$^{0.5}$)	33.1	33.1
Pressure (bar)	1.38	1.36
Droplets' velocity (V)(m/s)	12.9	12.3
median droplet diameter (d_{v50})(m)	0.0006	0.0005
Distribution width (γ)	2.3	2

2.5 The tested cases

Four types of tests were carried out to investigate the effect of different variables on the plume-sprinkler interactions. The total water volume flux on the ground was measured and the vertical gas velocity at various heights was also sampled.

The first test focused on the effect of water droplet size on the interaction between the plume and the sprinkler. Two different sizes of droplets were chosen and the results were compared in terms of droplet distribution in the air, water flux, and gas phase velocity. The two sizes are: large droplets 5 mm, and small droplets 0.05 mm. Unlike other cases (where the spray was initialized by "uniformSamplingSprinklerInjection" model which creates a polydispersed spray), the "coneInjection" model was used in this test to produce a uniform droplet size in the spray (monodispersed spray).

The second test was carried out to examine the effect of numerical resolution on the results, the three resolution parameters (grid size, time step, and particle injection rate) were varied and the error was calculated for each case to check how it changes.

The third conducted test checked the numerical results of water flux and gas phase velocity for cases with different plume velocities (between 0 and 3.7 m/s). A validation study was done by comparing the numerical results with the available experimental results (linear water flux along the configuration with the absence of the plume, and the delivered water flux in the position of the plume with different plume velocities).

The fourth test examined the effect of plume temperature, evaporation, and plume position on water flux on the ground. The temperature was changed from $298\,°K$ to $498\,°K$ and $698\,°K$. Also, Evaporation and heat transfer models were tuned on to see their effect using the same temperatures above. Additionally, the position of the plume was changed between 5 cm and 215 cm along the x axis.

The results were explained by appropriate figures, compared with each other's, discussed and illustrated as possible.

3 Results

A number of simulations were carried out to investigate the effect of the plume on the distribution of the droplets on the ground and the impact of the sprinkler on gas phase velocity. Therefore, the total mass of water inside each collector is calculated during the simulation time and the results were analysed. Also, the velocity of the gas phase is analysed on different heights.

3.1 Drop size effect

Before examining the effect of numerical parameters and figure out the change in results due to changes in plume characteristics, it is important to see the effect of water droplet size on the results. In this test, the "coneInjection" model, which produces a uniform droplets in all directions, was used. The cone angle was set to $90°$ to represent a hemisphere as if it is a sprinkler. Two different diameters were chosen: large droplets 5 mm and small droplets 0.05 mm. In both cases, the same mass flow rate was used; 0.64 kg/s.

Figure 10 (generated in ParaView) shows the velocity field for a vertical plane along the x-axis. It also shows the distribution of droplets in the domain for both cases.

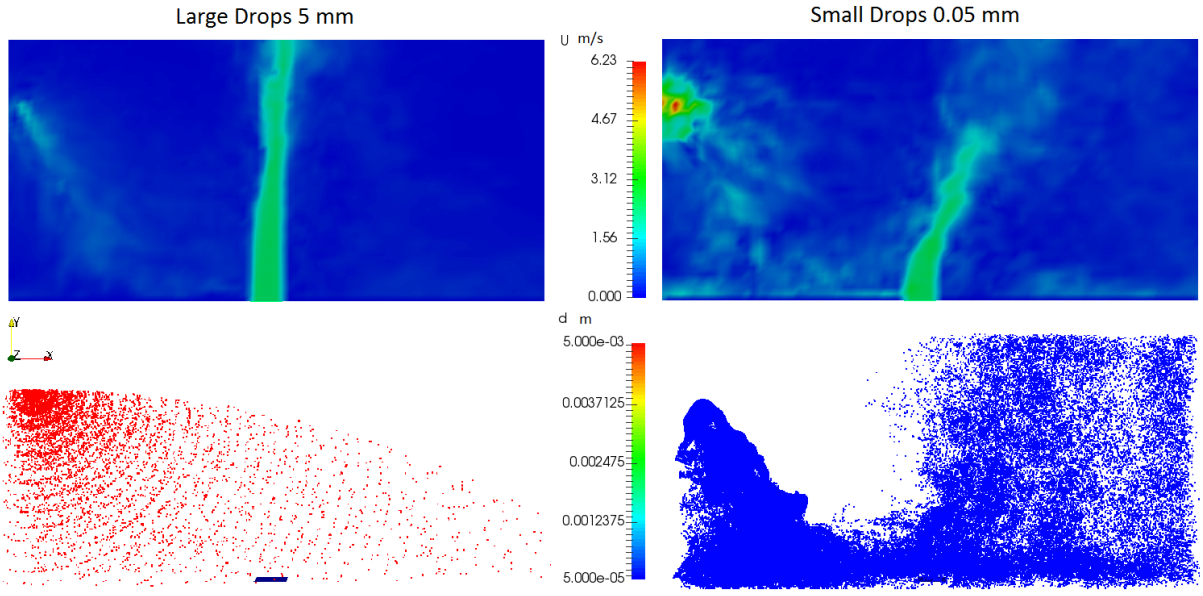

Figure 10 A comparison for gas phase velocity (up) and drops distribution (down) between large droplets 5 mm (left) and small droplets 0.05 mm (right)

It is noticeable from Figure 10 that small droplets are more capable of influencing the plume and effect its path. Also of notice the distribution of droplets in the domain; large droplets which have high momentum are not affected by the plume and their distribution is the same with or without a plume. While small droplets distribution is highly influenced by the plume and the majority of the drops are blown by the plume as they come in touch with it. Also,

large drops with high momentum are capable of reaching the farthest point of the domain, while small droplets have low momentum and as they are injected, the drag force pulls the drops into the ground.

Figure 11 shows the plot of the average velocity of the gas phase at height 1.5 m above the ground for both situations (large and small droplets) in three different cases (plume-only, sprinkler-only, and plume-sprinkler). It is noticeable that gas phase velocities in the two situations are distinct from each other. The large droplets have a small impact on the gas phase and the plume. The speed of the plume does not change significantly with large drops, while it is noticeable how it is influenced by small drops and its speed decreases significantly. The peak point of the velocity indicates the effect of the spray on the plume as it is bent, small droplets have a bigger effect than large droplets in bending the vertical path of the plume.

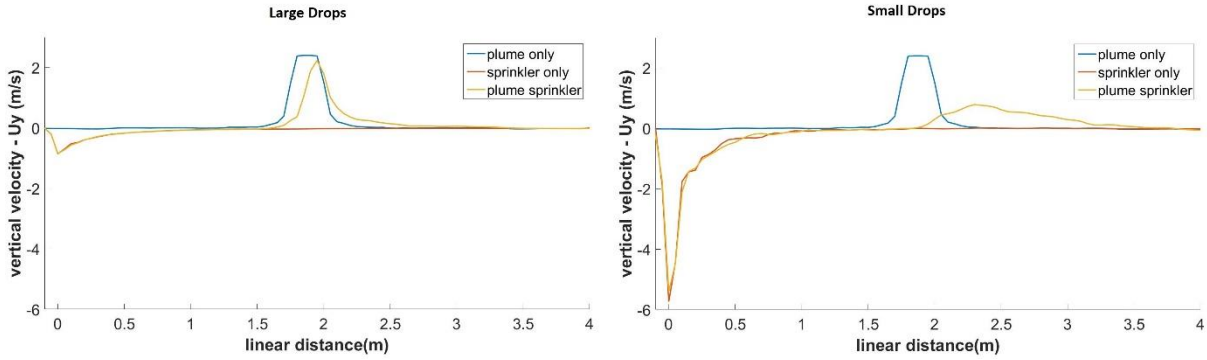

Figure 11 Gas phase velocity at height 1.5 m for large drops (left) and small drops (right) in three different cases

On the other hand, the volume flux on the ground changes between the small and large drops as seen in Figure 12. The volume flux for large droplets does not change a lot as the fraction (between the cases with a plume and without a plume) remains almost 1 along the domain. The volume flux in large droplets has its maximum under the sprinkler directly and it decreases gradually along the domain. While the volume flux fraction (between the cases with a plume and without a plume) in small drops varies along the domain and it is 0 in the plume position. Even the mass flow rate for both drop sizes is the same, the total volume flux on the ground for small droplets is much less than the total volume flux on the ground for large droplets as seen in the left figure.

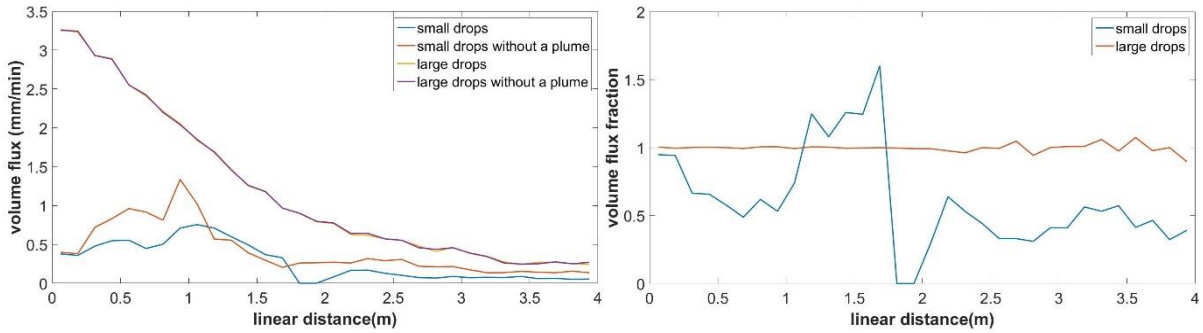

Figure 12 Volume flux on the ground accumulated from large droplets and small droplets with and without a plume (left) and volume flux fraction (the ratio between volume flux with a plume and volume flux without a plume in the same position) for small and large droplets (right)

3.2 Resolution study

Before analysing the change in sprinkler-plume interaction when plume speed, plume velocity, and plume temperature, are changed individually, it is important to estimate the numerical errors that happen due to the specific choice of spatial, temporal, and spray discretization.

It is known that the numerical error decreases as the resolution increases, but this accuracy comes at computational expenses. A smart choice of the resolution is important as it reduces the numerical error into acceptable levels without unnecessary computational expense. However, errors may also come from the assumptions made in each sub-model and solution algorithms. The chosen boundary conditions cause additional errors in accordance with the accuracy they have been specified at [9]. In the present work, only errors that come from resolution will be discussed.

Myers et al. [9] referred to a length scale and a time scale that are used to define non-dimensional resolution parameters in order to have an appropriate selection for the resolution to simulate sprinkler sprays. To investigate the resolution, a number of cases were done by changing grid cell size dx, time step dt, and the injection rate of particles $\dot{N}$, each at a time. In order to resolve the dispersion of the spray, the motion of the gas phase, and the interaction between them, it is important to resolve the smallest length scale, the fastest motion, and represent Lagrangian particles in every volume of interest.

The smallest characteristic length x_c and the grid cell size dx should have the relation shown in equation (9).

$$dx/x_c \ll 1 \qquad (9)$$

The maximum velocity U_c is identified to specify the time scale of interest $t_c = x_c/U_c$, then the time step and the time scale should have the relation shown in equation (10).

$$dt/t_c \ll 1 \qquad (10)$$

For an Eulerian numerical solution, global error will be first order accurate with dx and dt. The Lagrangian particles injected per time of interest per volume of interest should be much larger than one as shown in equation (11).

$$\frac{N \cdot t_c}{V_{spray}/x_c^3} \gg 1 \qquad (11)$$

The global error for Lagrangian particle injection rate will behave like a statistical standard error and go like $1/\sqrt{N \cdot}$.

A well-resolved case for each resolution parameter has been run and the parameter of interest was varied for each case to study the impact on global error. The smallest length scale is the equivalent diameter of the plume which is 0.219 m, the maximum velocity of interest is the drop injection velocity which is 12.3 m/s. So the smallest time scale is 0.0178 s. The volume of the spray is calculated approximately by assuming it is a cone with radius of 4 m (the spray throw) and height of 1.5 m (the sprinkler height), yielding a volume of $25\ m^3$. Table 4 shows the chosen resolution for each well resolved case.

Table 4 Resolution for the well-resolved simulations

Case	User settings		Resolution	
Spatial	dx (m)	0.02	dx/x_c	0.09
	dt (s)	0.001	dt/t_c	0.056
	N· (particles/s)	1,000,000	$N \cdot t_c/(V_{spray}/x_c^3)$	7
Temporal	dx (m)	0.025	dx/x_c	0.11
	dt (s)	0.0005	dt/t_c	0.028
	N· (particles/s)	10,000,000	$N \cdot t_c/(V_{spray}/x_c^3)$	74
Particle sampling	dx (m)	0.05	dx/x_c	0.23
	dt (s)	0.001	dt/t_c	0.056
	N· (particles/s)	10,000,000	$N \cdot t_c/(V_{spray}/x_c^3)$	74

The order of accuracy has been tested by varying grid cell size, time step, and particle injection rate independently. In each case the global error in the volume flux on the floor was compared to the resolution, where the error δ_x is defined as in equation (12).

$$\delta_x = \sqrt{\frac{\sum_{i=1}^{N}(f_{r,i} - f_{x,i})^2}{\sum_{i=1}^{N} {f_{r,i}}^2}} \qquad (12)$$

Where N is number of local measurements, $f_{r,i}$ is the true local measurement at location i, and $f_{x,i}$ is the tested local measurement at location i. In the following verification cases, this metric is used to compare the time-averaged volume flux.

3.2.1 Spatial resolution

To minimize error, the grid cell size dx, should be much smaller than the characteristic length scale x_c. Due to the large size of the domain and computational resource restrictions, this could not be realized in any except the well-resolved case and the fine cases. The cases run and the error in volume flux on the ground are shown in Table 5 and Figure 13. It is noticeable that the results' error is almost following the line of first order accuracy with space as hypothesized.

Table 5 Grid resolution cases

Case	dx (m)	x_c (m)	dx/x_c	Flux Error
Base	0.02	0.219	0.09	-
Very fine	0.025	0.219	0.11	8.9%
Fine	0.05	0.219	0.23	14.2%
Medium	0.08	0.219	0.36	19.2%
Coarse	0.12	0.219	0.55	22.9%
Very coarse	0.2	0.219	0.91	41.6%

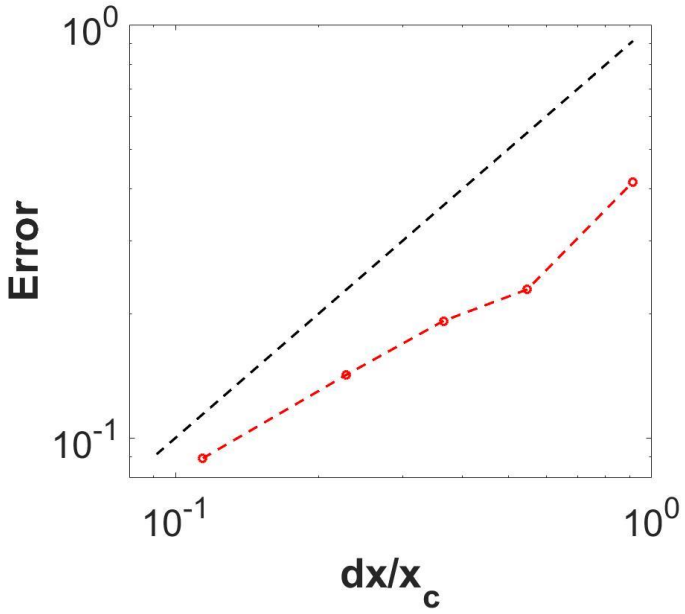

Figure 13 The impact on global error in volumetric flux as a function of grid resolution

3.2.2 Temporal resolution

To minimize error associated with the time evolution of the gas-phase and Lagrangian particle evolution equations the time step dt, should be much smaller than the characteristic time scale t_c. Because of the Courant number requirements, this time step will likely always be much smaller than time scale, but the medium and coarse cases where not that so. The cases run and the error in volume flux on the ground are shown in Table 6 and Figure 14. It is

noticeable that the results' error is not exactly following the line of first order accuracy with time as hypothesized. This happens because the maximum velocity of interest is high which requires a very small time step to be well resolved.

Table 6 Time step resolution cases

Case	dt (s)	t_c (s)	dt/t_c	Flux Error
Base	0.0005	0.0178	0.028	-
Fine	0.001	0.0178	0.0562	7%
Medium	0.005	0.0178	0.28	14%
Coarse	0.01	0.0178	0.56	16.1%

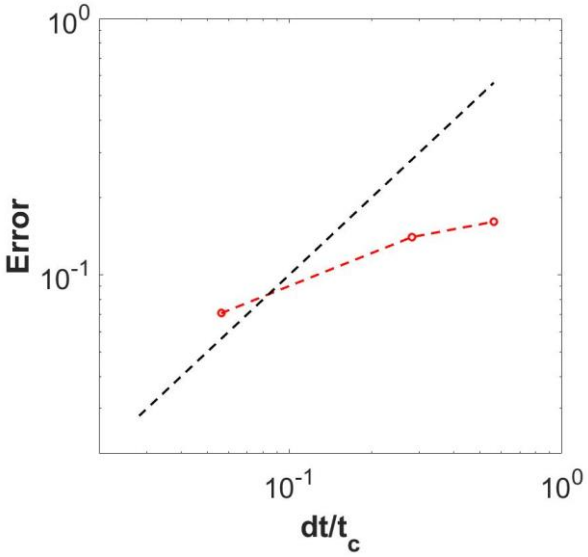

Figure 14 The impact on global error in volumetric flux as a function of time step resolution

3.2.3 Particle sampling resolution

For multiphase cases, as in plume-spray cases, a new unfamiliar error appears which is associated with particle injection. The sprinkler is polydispersed, therefore, a representative sample of the spray in each volume of interest each time of interest is needed. To accurately predict the gas phase conditions, it is necessary to have an accurate sampling of the spray because they interact with each other and therefore determine the spray trajectories and future gas conditions. Resolving the spray interactions over the timescale of interest is important to avoid errors in prediction even if the spray is statistically resolved over a long timescale [9].

Figure 15 and Figure 16 show the volume flux over time on two different locations (55 cm and 181 cm away from the sprinkler respectively). As the injection rate of particles decreases, the fluctuations increases and the global average also changes. It is also noticeable that farther from the sprinkler, the fluctuations in fine cases are less, this happens because the particles

in farther locations are larger and they are resolved better than the smaller particles near the sprinkler.

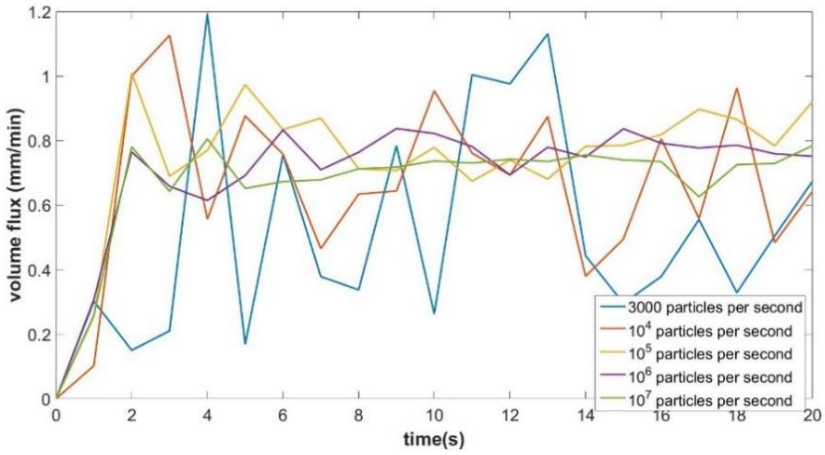

Figure 15 The volume flux over time at 55 cm away from sprinkler for different particle injection rates

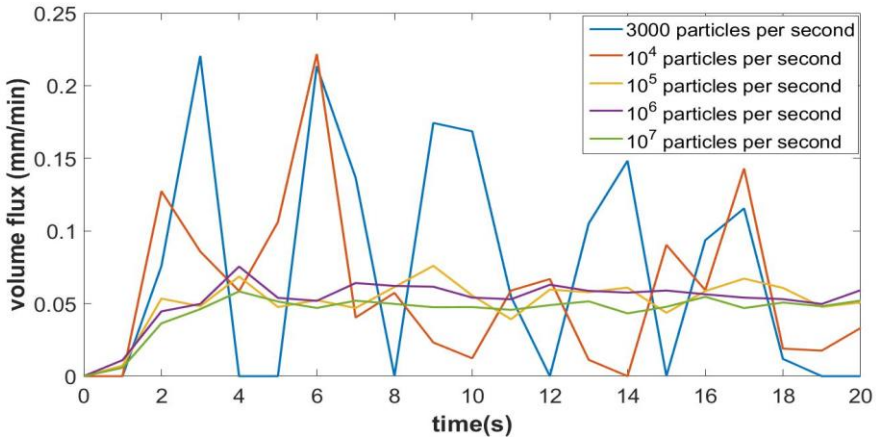

Figure 16 The volume flux over time at 181 cm away from sprinkler for different particle injection rates

An analysis of the global error is shown in Table 7 and Figure 17. It is noticeable that the error decreases as $1/\sqrt{N\cdot}$ as hypothesized. Because of the restriction of computational resources, the particles injected per time of interest per volume of interest are larger than 1 only for base and fine cases. The numbers less than 1 indicate that not every single volume of interest every time of interest has a particle inside it. This limited number of particles has a big impact on the error as seen in Table 7 for medium and coarser cases.

Table 7 Particle injection resolution cases

Case	$N\cdot$ (particle/s)	$t_c/(V_s/x_c^3)$ (s)	$N\cdot t_c/(V_s/x_c^3)$	Flux Error
Base	10,000,000	$7.14*10^{-6}$	74	-
Fine	1,000,000	$7.14*10^{-6}$	7	5.3%
Medium	100,000	$7.14*10^{-6}$	0.7	20.3%

Coarse	10,000	$7.14*10^{-6}$	0.07	43%
Very coarse	3000	$7.14*10^{-6}$	0.02	50.7%

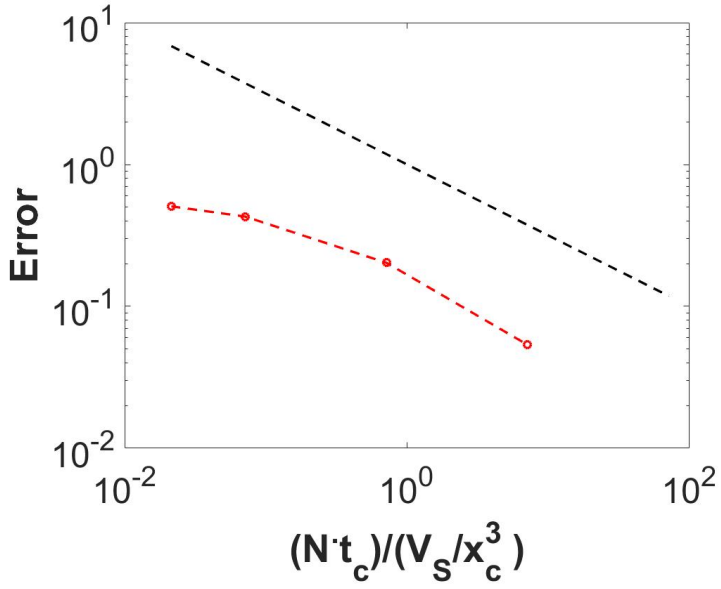

Figure 17 The impact on global error in volumetric flux as a function of particle injection resolution

3.3 Plume-sprinkler interaction

In this analysis, three changes were introduced individually to the plume to see their effects on the plume-sprinkler interaction. First, the speed of the plume was changed to see its effect on water flux on the ground. Second, the temperature of the plume was changed, then the evaporation and heat transfer models were activated in order to examine the effect of these changes on the water distribution on the ground. Third, the position of the plume was changed and the plume-sprinkler interaction was investigated. A comparison with experimental results is shown for the first case test. In all cases, the mesh is uniform and it has a grid spacing of 5 cm. The time step chosen is 0.001 s and particles injection rate is 10^6 particles/s.

3.3.1 Validation study

A number of experimental results are available through experiments done by Link [20], [21]. The water flux on the ground with the absence of a plume is measured through experiments, also the water flux in the position of the plume is measured at different plume velocities. These experimental results are used to validate the simulation results done for comparable cases.

3.3.1.1 Water flux without a plume

Before examining the effect of plume velocity on water flux, it is important to see the water flux pattern on the ground for a case without a plume.

A set of water flux results have been collected experimentally from a single sprinkler without a plume [20]. A comparison between the experiment and the simulation is seen in Figure 18. The two lines on the graph have a good agreement on all points except for the area around the peak where the simulation is over predicting the result. However, as the droplets in this area have small diameters, the results can be improved by increasing the resolution, and by that a better convergence can be caught on these points.

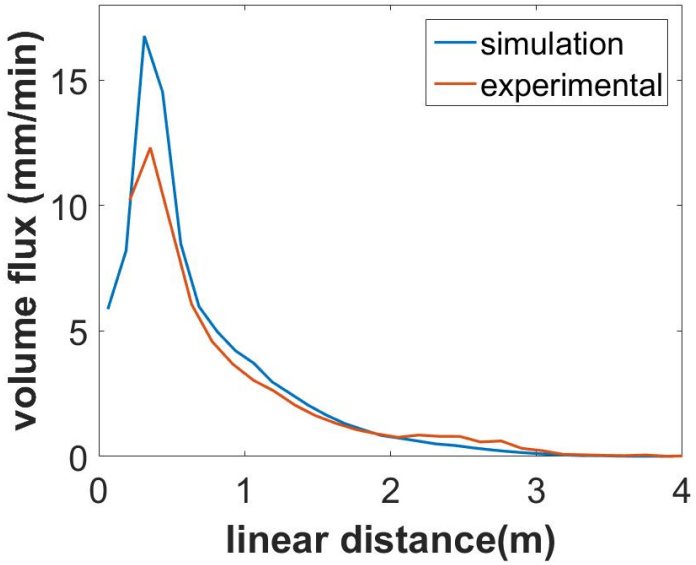

Figure 18 A comparison for water flux between the simulation and the experiment without a plume

3.3.1.2 Plume speed effect

As mentioned before, the velocity of the plume is 2.4 m/s for all other cases. However, in this analysis the velocity has been changed into different values between 1.4 and 3.7 m/s. The chosen values were identical to values from experiments.

In Figure 19 we can see the water volume flux on the ground for all the simulated cases. As expected, that volume flux in the position of the plume decreases as the velocity of the plume increases. The volume flux is noticeably lower for velocities over 2.4 m/s, because these plume velocities are higher than the terminal velocities of the drops and only individual large drops with terminal velocities higher than the plume's one are capable of penetrating it into the ground. Also, the distance between the plume and the sprinkler is relatively long, thus the trajectories of droplets toward the plume make the interaction region small and it mainly happens on one side of the plume which, eventually, makes more droplets to penetrate the plume into the ground.

A comparison between the performed simulations and experimental results [21] for water flux in the position of the plume is shown in Figure 20. As expected, the velocity increase leads to lower water flux inside the plume. In most cases, the simulation is over predicting the water flux, but in general the values are close in simulation and experiment except at high velocities

when the resolution should be increased in order to be able to predict the results quite well and have a good convergence compared with experimental data.

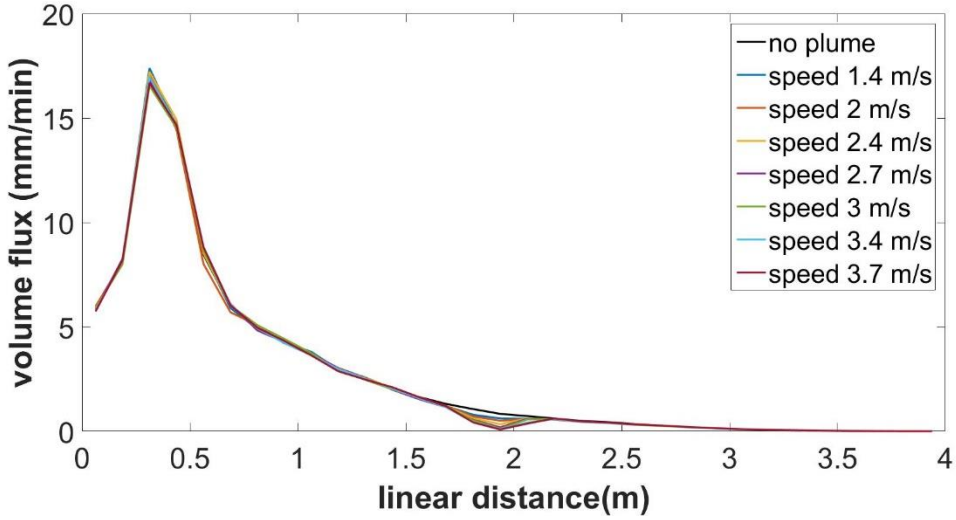

Figure 19 Water flux on the ground in all positions for different plume speeds

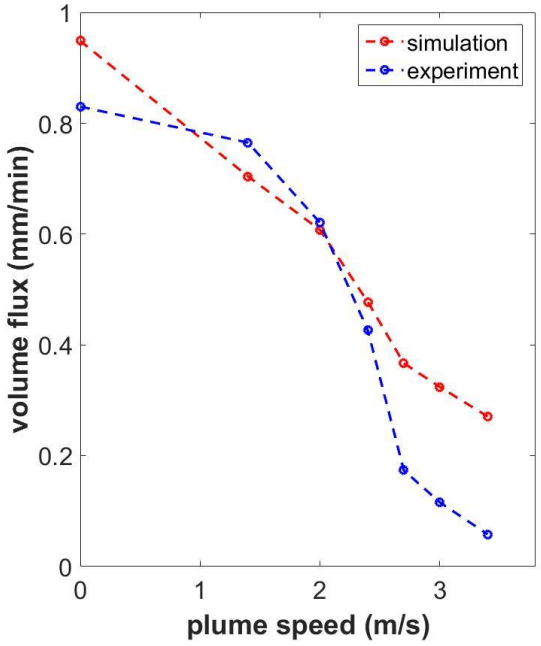

Figure 20 Water flux in the position of the plume against plume velocity for simulation and experiment

Figure 21 shows water flux fraction inside the plume against the velocity of it for simulations and experiment; the volume flux of each was normalized by the corresponding water flux of the case without a plume. The effect of large droplets having high terminal velocities can be seen for plume velocities higher than 2.4 m/s as the slope of water flux fraction is less after this velocity.

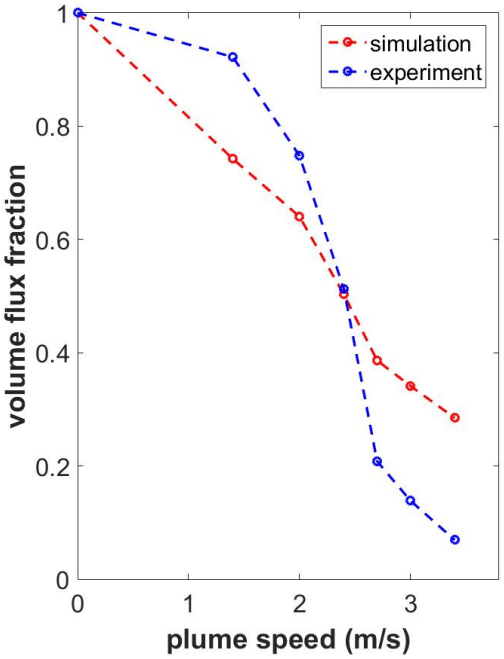

Figure 21 Water flux in the position of the plume for each plume velocity normalized by the water flux in the case without a plume

3.3.2 Additional plume changes

A natural progression of the study includes the change of the temperature and the position of the plume to see their effect on water flux. Even the experimental data are still not available for these cases, yet it is important to include them in this study in order to have a realistic effect of the plume temperature and to see how the interaction between the plume and the sprinkler changes as the position of the plume is changed.

3.3.2.1 Plume temperature effect

The temperature of the plume was changed from $298\ °K$ (the ambient temperature) to $498\ °K$ and $698\ °K$. The effect of evaporation was also tested by turning the evaporation and heat transfer models on and see the effect on water flux on the ground in all temperatures $298\ °K$, $498\ °K$ and $698\ °K$.

The volume flux in the ground for all cases is shown in Figure 22. It is noticeable that the volume flux pattern in all cases is almost the same. Therefore, we can say that the temperature and evaporation do not have a significant impact on the volume flux on the ground except the small change in the position of the plume.

Figure 23 shows the effect of temperature and evaporation on water flux in the position of the plume normalized by the flux in ambient temperature without evaporation. It is noticeable that the water flux increases as the temperature increases, this happens because the density of the gas decreases as temperature increases which leads to having lower plume momentum. As a result, water droplets are capable of penetrating the plume as the drops

have a higher momentum than the plume now. However, this trend does not rely only on density, because the velocity also increases in hot plumes due to buoyancy and therefore the total decrease in the momentum becomes less.

On the other hand, the evaporation has also an effect on the results. As seen in Figure 23, the water flux is less than the cases were the evaporation was turned off. As expected, the evaporation increases as the temperature increases. However, the difference is not big because the droplets pass fast through the plume and they do not have enough time to evaporate. In addition, in this area the droplets are big and they have a small surface area to volume ratio, therefore, they are less affected by evaporation.

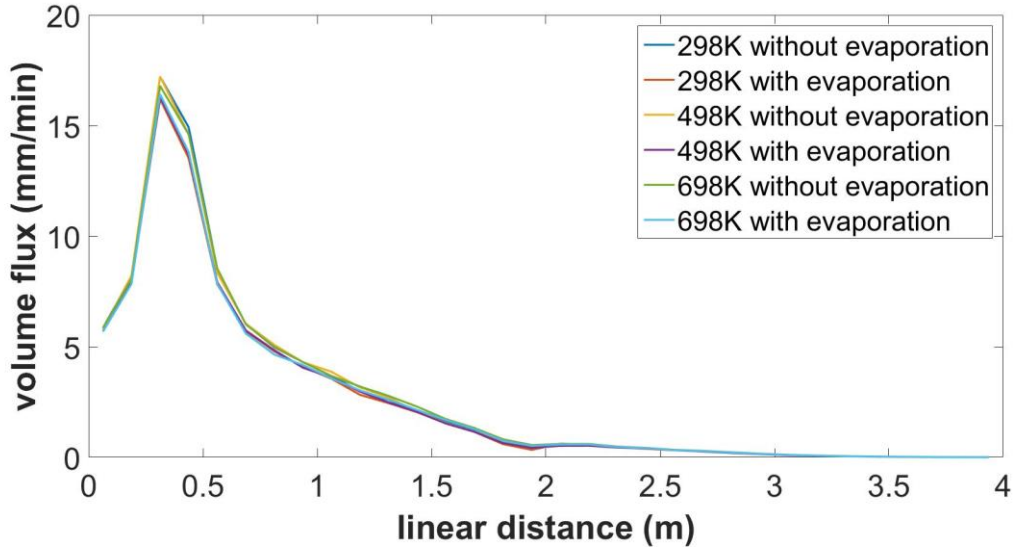

Figure 22 Water flux on the ground as a function of linear distance for different plume temperature with and without evaporation

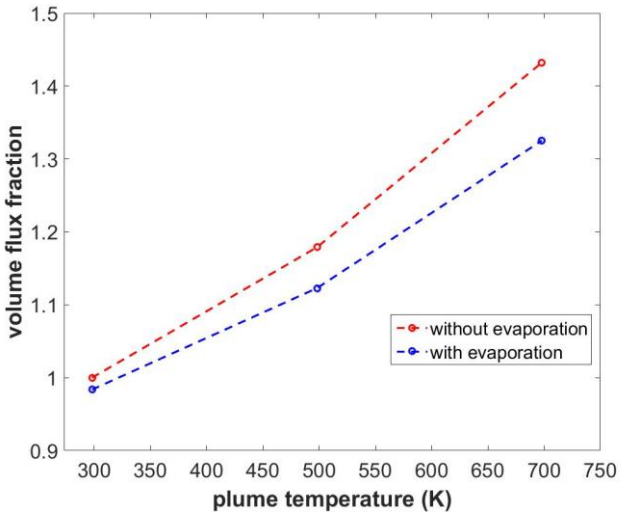

Figure 23 The effect of temperature and evaporation on water flux normalized by the water flux in ambient temperature without evaporation

3.3.2.2 Plume position effect

In this analysis, plume centre position was changed along the x-axis between 0.05 and 2.15 m in order to see the change in water flux. Figure 24 shows the water flux on the ground for all cases. It is noticeable that in the plume position the water flux is the lowest compared to other areas along the domain.

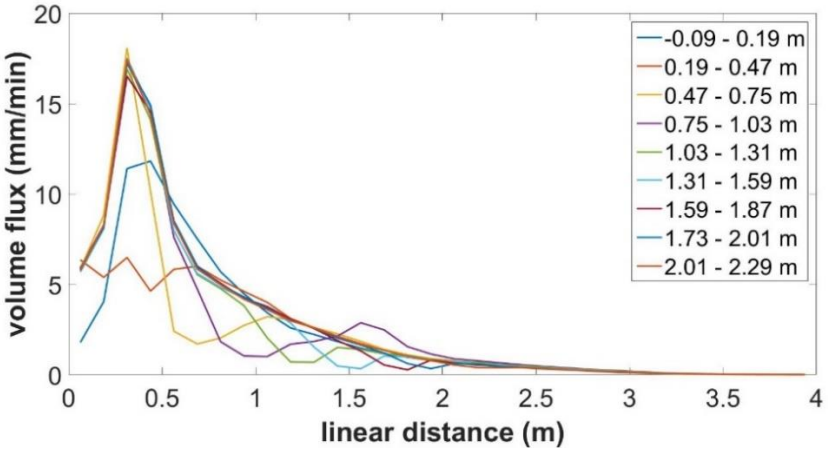

Figure 24 Plume position effect on water volume flux pattern

Figure 25 shows how the delivered flux on the ground changes with plume position (all normalized by the delivered flux in the same position without a plume). It is noticeable that the plume decreases the delivered flux into about 30-40% of its original value except points farther than 1.75 m from the sprinkler position where the delivered flux is 50-60% of its original value, this happens because droplets in farther positions have bigger diameters and are capable of penetrating the plume in this position. In addition, in farther positions the trajectories of the droplets impose a small interaction area with the plume.

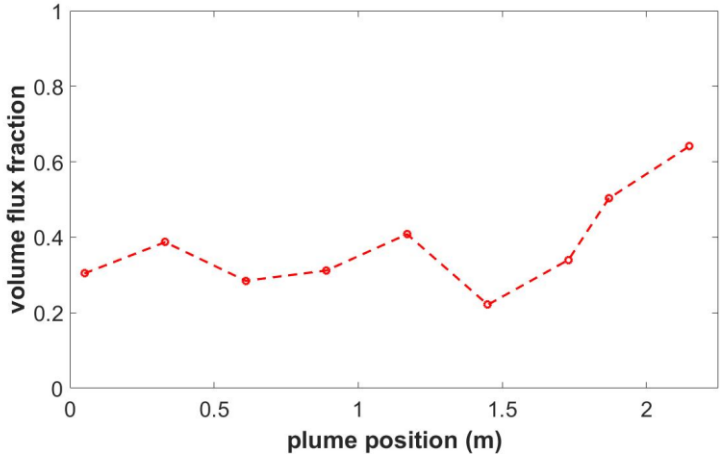

Figure 25 The water flux in different plume position normalized by the water flux delivered into the same position without the presence of the plume

3.3.3 Spray-plume effect on gas velocity

Despite the delivered volume flux from the sprinkler to the ground, it is also of interest to analyse the change in gas velocity along the domain. This velocity indicates the movement direction in the air as it is affected by the plume, the sprinkler or both of them. The average values of the vertical velocity along three horizontal lines in x-axis direction located 0.5, 1, and 1.5 m above the floor was measured in FireFOAM. The average vertical velocity of a case with a plume only is shown in Figure 26, for a case with a sprinkler only is shown in Figure 27, and for a case with a plume-sprinkler is shown in Figure 28.

As seen in Figure 26, the vertical velocity decreases slightly with height, while plume width increases with height. Figure 27 shows that the sprinkler has a big impact on the quiescent gas as the droplets drag the air downward especially in the region 0.5 m below the sprinkler (1 m from the ground). This downward gas movement disperses as we move farther from the sprinkler. It is noticeable from Figure 28 that the sprinkler has an effect on the plume which makes it bends to the right (away from the sprinkler) as the gas rises up. Also, the speed of the plume decreases significantly by the effect of the sprinkler.

In order to compare the three cases together, Figure 29 shows the vertical velocities for the cases but only for a one-meter-height horizontal line across the domain. Here, the effect on the plume is apparent as its velocity is significantly decreased and the peak of the speed indicates how the plume is bent.

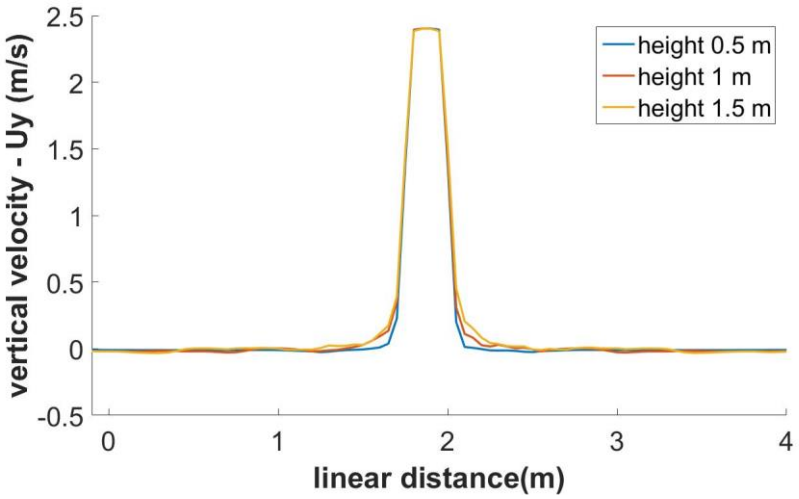

Figure 26 Average vertical velocity for a plume-only case at three different heights

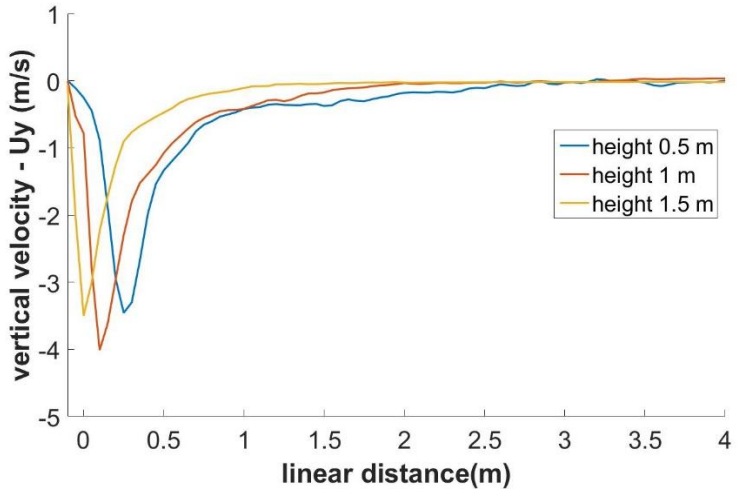

Figure 27 Average vertical velocity for a sprinkler-only case at three different heights

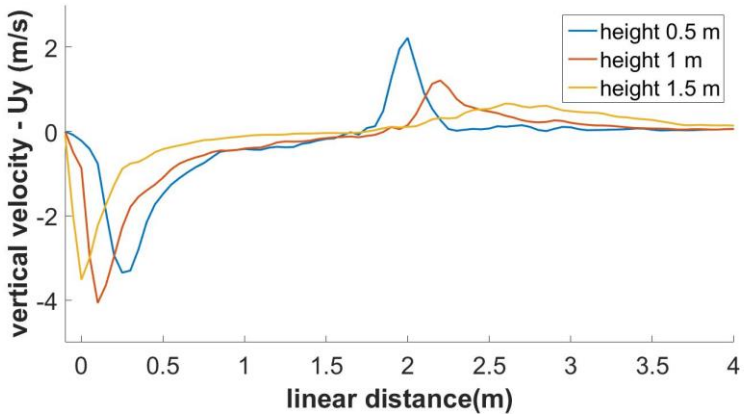

Figure 28 Average vertical velocity for a plume-sprinkler case at three different heights

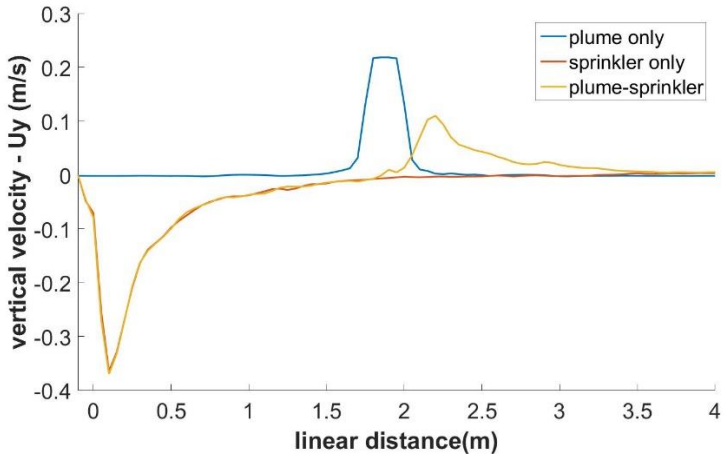

Figure 29 Average vertical velocity at 1 m height for the cases (plume only - sprinkler only - plume-sprinkler)

4 Discussion

The presented cases above examined different changes in the conditions of a plume-sprinkler case. Both of the spray's and the plume's parameters were changed in this study.

The monodispersed cases, where two different sizes of droplets were injected, showed how easily large droplets penetrate the plume and how they are able to deliver water in the position of the plume (Figure 12), thus large droplets are able to wet the combustible materials and restrain fire growth (fuel cooling). On the other hand, small droplets employ their large spatial volume (effective dispersion) in blowing the plume (Figure 10 and Figure 11). In addition, it is know that in the presence of flames, small droplets are not only able to reduce radiation, but also they evaporate quickly because of the high surface area to volume ratio they have, and as droplets evaporate they replace oxygen and cool gas temperature (flame cooling) [3], [7].

The resolution study showed how significantly the numerical parameters (grid size, time step, and particle injection rate) affect the results of the simulation. It was evident that a good resolution is required to have reasonable results. However, increasing the resolution to unnecessary levels has a significant impact on the computational expenses. It was also shown that the total error does not change linearly with resolution, thus an intelligent choice of all parameter at once is essential in reducing the computational cost without losing the accurate results [9].

Because this study focuses on the interaction between the sprinkler and the plume in a relatively large domain and due to the computational restrictions, the chosen resolution parameters were not resolved quite well as they should be if we study the plume or the sprinkler individually. However, the results were generally good and they showed a valid agreement with the available experimental data [20], [21]. Nevertheless, the resolution has to be better in order to have a good convergence in all parameters.

The validation study of the numerical results in the absence of the plume showed an excellent agreement with experiments (Figure 18). Only points near the sprinkler showed a small deviation, but this divergence can be rectified by better resolution which is able to catch the behaviour of small droplets. Also, in the cases of different plume velocities, the numerical results were close to experimental ones (Figure 21). However, for the same resolution reason, the simulations with high plume velocities showed a small variance with experiments.

The plume velocity effect was noticeable in the tested cases; as the volume flux of water decreases when the velocity increases. Also, it was noticeable that when the velocity of the plume is higher than the terminal velocities of droplets, the volume flux on the ground decreases significantly [21].

The temperature change showed that the water flux on the ground increases as the temperature increase (Figure 23). Positioning the plume far from the sprinkler made the

trajectories of the droplets intact until they reach the area around the plume, therefore, the interaction region between the plume and the spray is small and only happens from one side of the plume. As a result, the effect of buoyancy (which makes the plume faster in high temperatures) was less than the effect of density (which makes the momentum of air lower in high temperatures), thus more water was delivered to the position of the plume in these cases.

On the other hand, the evaporation model showed that there is a small effect on the total volume flux on the ground. This effect increases as the temperature increases. However, at a very high temperature like $698\,°K$ the evaporation effect is less than 10% change from the original value without evaporation. This indicates that the evaporation does not have a big influence on the total volume flux and the sprinkler does its function well in the presence of high temperature.

Changing the position showed that the plume affects the water flux delivery to the area around the plume, but generally the efficiency of delivering water to the plume position is around 30-60% than its value without a plume (Figure 24 and Figure 25). The water flux fraction in the position of the plume increases far from the sprinkler because large droplets in farther positions are more capable of penetrating the plume than small droplets close to the sprinkler.

The analysis of gas phase velocity showed that the sprinkler's spray has a considerable influence on the gas phase and the plume. The quiescent gas under the sprinkler is influenced to have a high downward velocity when the sprinkler is activated. Also, the velocity of the plume decreases significantly under the effect of the sprinkler and the vertical path of the plume is bent as well [1], [14]. Due to the large distance that splits the plume and the sprinkler in this study, the effect of the sprinkler on the plume was noticeable quite well, while the effect of the plume on the spray near the sprinkler was negligible.

5 Conclusion

The present study was conducted to investigate the interaction between a fire sprinkler and a plume. A number of numerical simulations were carried out to see how changes in sprinkler's and plume's characteristics affect water flux on the ground, and also to see how the gas phase velocity is changed as a result of this interaction. Additionally, some of the simulations were validated with available experimental data.

First, two droplet sizes were used in the spray to see the difference between them in terms of droplets dispersion, water volume flux, gas phase velocity and the effect on the plume itself. It has been found that large droplets have a higher ability than small droplets in delivering water into the ground, while small droplets are more able to influence the gas phase and the path of the plume. Also, small droplets were found to lose their momentum quickly compared to large droplets.

On the other hand, the numerical parameters (such as grid size, time step, and particles injection rate) were found to have a significant effect on simulation time, thus the resolution has to be chosen carefully. A balance between the numerical costs and the fidelity of the results should be achieved to have an acceptable error value.

Plume velocity was discovered to influence water flux on the ground especially when this velocity exceeds the terminal velocity of the majority of the droplets. The numerical results were validated through experimental data and it has been concluded that they have a good agreement when the numerical parameters are resolved well.

Additional numerical simulations were carried out to see how the temperature of the plume, and droplets' evaporation change the volume flux on the ground. Surprisingly, the water flux was found to increase when the temperature of the plume was increased. The activation of the evaporation model showed that it has an inconsiderable influence on the amount of delivered water which corroborates the usage of the cold plume in experiments.

Finally, changing the position of the plume showed that the delivered water into the plume is about 30-60% of its original value when there is no plume. It also enhanced the fact that large droplets far from the sprinkler are more able to penetrate the plume than small droplets.

Potential future studies would be additional investigations for the actual size of the droplets, and the density of the spray both experimentally and numerically. Also, introducing realistic flames instead of the plume makes the results more reliable. At an advanced step, coupling the flame with the new extinction feature that has been added to FireFOAM should be used in order to have a comprehensive understanding of the interaction between the sprinkler and the fire. All numerical results would be questionable until they are validated through equivalent experiments.

Acknowledgment

This project is part of the international master in fire safety engineering; IMFSE. I would like to thank all professors in the Universities of Edinburgh (UK), Lund (Sweden) and Gent (Belgium) for the knowledge they offered me in all semesters I spent in these universities. A special thank for all my fellow graduate students for the friendships we made.

I would like to thank the University of Maryland (USA) for the opportunity they gave me in spending the last semester doing the thesis in the Department of Fire Protection Engineering. I also would like to thank all people in the department for their friendliness.

I would like to thank my supervisor in this thesis, Professor Arnaud Trouvé for the opportunity he gave me to do this interesting study and for the endless support he gave me during the whole semester. Thank you for your advice and your guidance that helped in having a better study.

I would like to thank Professor Andre Marshall for the efforts he made in supervising the experimental measurements.

I acknowledge all the invaluable help from PhD students in the department. Special thanks to Taylor Myers for his advice and comments on all parts of this study. Discussions with Eric Link are also highly acknowledged. Help and encourage from Salman Verma and Cong Zhang are highly appreciated.

References

[1] J. A. Schwille, "A Simplified Model of the Effect of a Fire Sprinkler Spray on a Buoyant Fire Plume," *J. Fire Prot. Eng.*, vol. 16, no. 2, pp. 131–153, May 2006.

[2] X. Zhou, S. P. D'Aniello, and H.-Z. Yu, "Spray characterization measurements of a pendent fire sprinkler," *Fire Saf. J.*, vol. 54, pp. 36–48, Nov. 2012.

[3] D. J. Rasbash, "The extinction of fire with plain water: a review," *Fire Saf. Sci.*, vol. 1, pp. 1145–1163, 1986.

[4] S. Vilfayeau, T. Myers, A. W. Marshall, and A. Trouvé, "Large eddy simulation of suppression of turbulent line fires by base-injected water mist," *Proc. Combust. Inst.*, vol. 36, 2016.

[5] T. M. Myers and A. W. Marshall, "A Description of the Initial Fire Sprinkler Spray," *Submitted. Fire Saf. J.*, 2016.

[6] N. Ren and A. W. Marshall, "Characterizing the initial spray from large Weber number impinging jets," *Int. J. Multiph. Flow*, vol. 58, pp. 205–213, Jan. 2014.

[7] N. Ren, H. R. Baum, and A. W. Marshall, "A comprehensive methodology for characterizing sprinkler sprays," *Proc. Combust. Inst.*, vol. 33, no. 2, pp. 2547–2554, Jan. 2011.

[8] A. Marshall, "Unraveling Fire Suppression Sprays," *Fire Saf. Sci.*, vol. 10, pp. 61–75, 2011.

[9] T. Myers, A. Trouvé, and A. Marshall, "Resolving Sprinkler Spray Dispersion in FireFOAM," *In-Preperation*, 2016.

[10] H. Z. Yu, "Investigation of spray patterns of selected sprinklers with the FMRC drop size measuring system," *Fire Saf. Sci.*, vol. 1, pp. 1165–1176, 1986.

[11] X. Zhou and H.-Z. Yu, "Experimental investigation of spray formation as affected by sprinkler geometry," *Fire Saf. J.*, vol. 46, no. 3, pp. 140–150, Apr. 2011.

[12] J. F. Widmann, "Phase Doppler interferometry measurements in water sprays produced by residential fire sprinklers," *Fire Saf. J.*, vol. 36, no. 6, pp. 545–567, 2001.

[13] B. R. Morton, G. Taylor, and J. S. Turner, "Turbulent gravitational convection from maintained and instantaneous sources," in *Proceedings of the Royal Society of London A: Mathematical, Physical and Engineering Sciences*, 1956, vol. 234, pp. 1–23.

[14] S. Nam, "Development of a computational model simulating the interaction between a fire plume and a sprinkler spray," *Fire Saf. J.*, vol. 26, no. 1, pp. 1–33, Feb. 1996.

[15] S. Nam, "Numerical simulation of the penetration capability of sprinkler sprays," *Fire Saf. J.*, vol. 32, no. 4, pp. 307–329, 1999.

[16] J. Hua, K. Kumar, B. C. Khoo, and H. Xue, "A numerical study of the interaction of water spray with a fire plume," *Fire Saf. J.*, vol. 37, no. 7, pp. 631–657, 2002.

[17] "fireFoam-dev," *GitHub*. [Online]. Available: https://github.com/fireFoam-dev. [Accessed: 08-Apr-2016].

[18] "OpenFOAM® | Open Source CFD | The OpenFOAM Foundation." [Online]. Available: http://www.openfoam.org/. [Accessed: 08-Apr-2016].

[19] D. Souvandy, "Sprinkler modeling with FireFOAM," Aix Marseille University (Internship at the University of Maryland), 2015.

[20] E. D. Link, S. J. Jordan, T. M. Myers, P. B. Sunderland, and A. W. Marshall, "Spray Dispersion Measurements of a Sprinkler Array," *Proc. Combust. Inst.*, vol. 36, 2016.

[21] E. D. Link, T. M. Myers, A. C. Trouvé, and A. W. Marshall, "Regimes of Fire Suppression Spray Penetration," presented at the 2016 Spring Technical Meeting Eastern States Section of the Combustion Institute, Princeton University, 2016.

[22] T. Myers, S. Vilfayeau, D. Souvandy, and A. Trouvé, “Verification of Spray Modeling in FireFOAM,” *In-Preperation*, 2016.
[23] “OpenFOAM® Documentation.” [Online]. Available: http://www.openfoam.org/docs/. [Accessed: 20-Apr-2016].

Appendix

An example of the input file “reactingCloud1Properties”

```
/*--------------------------------*- C++ -*----------------------------------*\
| =========                 |                                                 |
| \\      /  F ield         | OpenFOAM: The Open Source CFD Toolbox           |
|  \\    /   O peration     | Version:  2.2.x                                 |
|   \\  /    A nd           | Web:      www.OpenFOAM.org                      |
|    \\/     M anipulation  |                                                 |
\*---------------------------------------------------------------------------*/
FoamFile
{
    version     2.0;
    format      ascii;
    class       dictionary;
    location    "constant";
    object      reactingCloud1Properties;
}
// * * * * * * * * * * * * * * * * * * * * * * * * * * * * * * * * * * * * //
solution
{
    active          true;
    coupled         true; // true;
    transient       yes;
    cellValueSourceCorrection on;
    sourceTerms
    {
        schemes
        {
            rho             explicit 1;
            U               explicit 1;
            Yi              explicit 1;
            h               explicit 1;
            radiation       explicit 1;
        }
```

```
    }
    interpolationSchemes
    {
        rho             cell;
        U               cellPoint;
        thermo:mu       cell;
        kappa           cell;
        T               cell;
        Cp              cell;
        p               cell;
    }
    integrationSchemes
    {
        U               Euler;
        T               analytical;
    }
}
constantProperties
{
    parcelTypeId     1;
    rhoMin           1e-15;
    TMin             200;
    pMin             1000;
    minParticleMass 1e-15;
    rho0             1000;
    T0               300;
    Cp0              4187;
    youngsModulus    1e9;
    poissonsRatio    0.35;
    epsilon0         1;
    f0               0.5;
    Pr               0.7;
    Tvap             273;
    Tbp              373;
```

```
    constantVolume  false;
}
subModels
{
    injectionModels
    {
        #include "XXXProperties"
    }
    compositionModel singlePhaseMixture;
    particleForces
    {
        sphereDrag;
        gravity;
    }
    dispersionModel none;
    surfaceFilmModel none;
    radiation       off;
    patchInteractionModel standardWallInteraction;
    stochasticCollisionModel none;
    heatTransferModel none;
    phaseChangeModel none;
    postProcessingModel none;
    standardWallInteractionCoeffs
    {
        type           escape;  //stick,escape,rebound
    }
    ranzMarshallCoeffs
    {
        // thermal shielding
        BirdCorrection  true;
    }
    patchPostProcessingCoeffs
    {
```

```
    maxStoredParcels    5000;
    patches
    (
        sides
        outlet
        base
    );
}
singlePhaseMixtureCoeffs
{
phases
(
    liquid
    {
        H2O 1;
    }
);
}
liquidEvaporationCoeffs
{
    enthalpyTransfer enthalpyDifference;

    activeLiquids
    (
        H2O
    );
}
thermoSurfaceFilmCoeffs
{
    interactionType absorb;
    deltaWetThreshold 0.0001;
    Adry            2630;
    Awet            1320;
    Cf              0.6;
```

```
        splashParcelPDF
        {
            pdfType          uniform;
            uniformPDF
            {
                minValue        1e-04;
                maxValue        1e-04;
            }
        }
    }
}
cloudFunctions
{
    particleCollectorFmg
    {

        type            particleCollectorFmg;
        mode            polygon;
        polygons
        (
//(( lowestX  Y  lowestZ) (lowestX  Y  highestZ) (highestX Y  highestZ) (highestX  Y  l
owestZ))
(( 0.000 0.010 -0.050) (0.000 0.010 0.050) (0.125 0.010 0.050) (0.125 0.010 -0.050)) // pa
n 1
(( 0.125 0.010 -0.050) (0.125 0.010 0.050) (0.250 0.010 0.050) (0.250 0.010 -0.050)) // pa
n 2
(( 0.250 0.010 -0.050) (0.250 0.010 0.050) (0.375 0.010 0.050) (0.375 0.010 -0.050)) // p
an 3
(( 0.375 0.010 -0.050) (0.375 0.010 0.050) (0.500 0.010 0.050) (0.500 0.010 -0.050)) // p
an 4
(( 0.500 0.010 -0.050) (0.500 0.010 0.050) (0.625 0.010 0.050) (0.625 0.010 -0.050)) // p
an 5
(( 0.625 0.010 -0.050) (0.625 0.010 0.050) (0.750 0.010 0.050) (0.750 0.010 -0.050)) // p
an 6
(( 0.750 0.010 -0.050) (0.750 0.010 0.050) (0.875 0.010 0.050) (0.875 0.010 -0.050)) // p
an 7
(( 0.875 0.010 -0.050) (0.875 0.010 0.050) (1.000 0.010 0.050) (1.000 0.010 -0.050)) // pa
n 8
```

((1.000 0.010 -0.050) (1.000 0.010 0.050) (1.125 0.010 0.050) (1.125 0.010 -0.050)) // PAN 9

((1.125 0.010 -0.050) (1.125 0.010 0.050) (1.250 0.010 0.050) (1.250 0.010 -0.050)) // PAN 10

((1.250 0.010 -0.050) (1.250 0.010 0.050) (1.375 0.010 0.050) (1.375 0.010 -0.050)) // PAN 11

((1.375 0.010 -0.050) (1.375 0.010 0.050) (1.500 0.010 0.050) (1.500 0.010 -0.050)) // PAN 12

((1.500 0.010 -0.050) (1.500 0.010 0.050) (1.625 0.010 0.050) (1.625 0.010 -0.050)) // PAN 13

((1.625 0.010 -0.050) (1.625 0.010 0.050) (1.750 0.010 0.050) (1.750 0.010 -0.050)) // PAN 14

((1.750 0.010 -0.050) (1.750 0.010 0.050) (1.875 0.010 0.050) (1.875 0.010 -0.050)) // PAN 15

((1.875 0.010 -0.050) (1.875 0.010 0.050) (2.000 0.010 0.050) (2.000 0.010 -0.050)) // PAN 16

((2.000 0.010 -0.050) (2.000 0.010 0.050) (2.125 0.010 0.050) (2.125 0.010 -0.050)) // PAN 17

((2.125 0.010 -0.050) (2.125 0.010 0.050) (2.250 0.010 0.050) (2.250 0.010 -0.050)) // PAN 18

((2.250 0.010 -0.050) (2.250 0.010 0.050) (2.375 0.010 0.050) (2.375 0.010 -0.050)) // PAN 19

((2.375 0.010 -0.050) (2.375 0.010 0.050) (2.500 0.010 0.050) (2.500 0.010 -0.050)) // PAN 20

((2.500 0.010 -0.050) (2.500 0.010 0.050) (2.625 0.010 0.050) (2.625 0.010 -0.050)) // PAN 21

((2.625 0.010 -0.050) (2.625 0.010 0.050) (2.750 0.010 0.050) (2.750 0.010 -0.050)) // PAN 22

((2.750 0.010 -0.050) (2.750 0.010 0.050) (2.875 0.010 0.050) (2.875 0.010 -0.050)) // PAN 23

((2.875 0.010 -0.050) (2.875 0.010 0.050) (3.000 0.010 0.050) (3.000 0.010 -0.050)) // PAN 24

((3.000 0.010 -0.050) (3.000 0.010 0.050) (3.125 0.010 0.050) (3.125 0.010 -0.050)) // PAN 25

((3.125 0.010 -0.050) (3.125 0.010 0.050) (3.250 0.010 0.050) (3.250 0.010 -0.050)) // PAN 26

((3.250 0.010 -0.050) (3.250 0.010 0.050) (3.375 0.010 0.050) (3.375 0.010 -0.050)) // PAN 27

((3.375 0.010 -0.050) (3.375 0.010 0.050) (3.500 0.010 0.050) (3.500 0.010 -0.050)) // PAN 28

((3.500 0.010 -0.050) (3.500 0.010 0.050) (3.625 0.010 0.050) (3.625 0.010 -0.050)) // PAN 29

```
(( 3.625 0.010 -0.050) (3.625 0.010 0.050) (3.750 0.010 0.050) (3.750 0.010 -0.050)) //
PAN 30

(( 3.750 0.010 -0.050) (3.750 0.010 0.050) (3.875 0.010 0.050) (3.875 0.010 -0.050)) // P
AN 31

(( 3.875 0.010 -0.050) (3.875 0.010 0.050) (4.000 0.010 0.050) (4.000 0.010 -0.050)) // P
AN 32

        );

        NORMAL          (0 -1 0);

        NEGATEPARCELSOPPOSITENORMAL NO;

        SURFACEFORMAT   VTK;

        RESETONWRITE    YES;

        LOG             YES;

        REMOVECOLLECTED YES;

    }

}

// ************************************************************************* //
```

An example of the input file "XXXProperties"

```
/*---------------------------------*- C++ -*----------------------------------*/

    UNIFORMSAMPLINGSPRINKLERINJECTION // UNIFORM

    {

        TYPE UNIFORMSAMPLINGSPRINKLERINJECTION; // UNIFORM

        LOOKUPTABLECOEFFS

        {

            // SAMPLE SIZE SHOULD IDEALLY NOT BE LARGER THAN THE NUMBER OF ELEMENTS IN T
HE LOOKUP TABLE

            SAMPLESIZE      500; // PER SPRINKLER, PER INJECTION TIME

            TABLEDIRECTORY  TABLE_XXX;

        }

        SOI             0.0;

        DURATION        20; //

        PARCELSPERSECOND 1000000;  // PER ONE SPRINKLER

        POSITIONLIST

            (

                (  0.0 1.5 0.0)

            );
```

```
        direction       ( 0 -1 0 );
        armDirection    ( 0  0  1);
        radiusToSprinkler 0.05; //m
        rtiCoeffs
        {
            active              false;
            RTI                 27.604; // (m s)^0.5  // average of 45-55 (ft s)^0.5
            C                   0.692; // (m/s)^0.5  // average of 0.7-1.81 (ft / s)^0.5
            initialTemperature  298.15;
            activationTemperature 344.26; // K  // average of 155-165 deg F
        // to convert RTI from (ft s )^0.5 to (m s)^0.5 square the value, multiply by 0.3
048, and take the sqrt
        // to convert C from (ft / s)^0.5 to (m/s)^0.5 square the value, multiply by 0.3
048, and take the sqrt
        }
        // begin section not used anywhere
            massTotal       -1;
            parcelBasisType mass;
        // end section not used anywhere
    }
```

An example of the input file “lookup.foam.header”

```
FoamFile
{
    version     2.0;
    format      ascii;
    class       dictionary;
    location    "constant";
    object      lookupTableInjection;
}
pressure    1.36; // pressure (bar),  19.6(psi)
kFactor     33.1; // kFactor (lpm/bar^0.5),   2.3 (gpm/psi^0.5)
radius      0.05; // radius (m)
nAzi        360; // azimuthal angles
nEle        91; // elevation angles
```